ELSEVIER

Contents lists available at ScienceDirect

Journal of Catalysis

journal homepage: www.elsevier.com/locate/jcat



Control of surface reactivity towards unsaturated C—C bonds and H over Ni-based intermetallic compounds in semi-hydrogenation of acetylene



Yuanjun Song, Siris Laursen*

Department of Chemical and Biomolecular Engineering, University of Tennessee - Knoxville, Knoxville 37996, USA

ARTICLE INFO

Article history: Received 5 August 2018 Revised 16 February 2019 Accepted 17 February 2019 Available online 12 March 2019

Keywords:
Intermetallic compounds
Non-noble metal catalyst
Surface chemistry
Unsaturated C—C bonds
Electronic effect
Ensemble effect
Semi-hydrogenation
DFT

ABSTRACT

Intermetallic compounds composed of transition metals and semimetals or post-transition metals have been shown to exhibit elevated selectivity in olefins and aromatics production and other reactions that require control of C=C activation and functionalization. The vast number of element combinations available for intermetallic compound production necessitates down-selecting to isolate catalytically useful compositional spaces. In this study, we have investigated the semi-hydrogenation of acetylene over isoelectronic intermetallic compounds composed of nickel and the boron group elements at a bulk stoichiometry of 1:1. We have isolated that orbital overlap between IMC constituent elements tracks well with the nature of their bulk bonding, surface reactivity, and catalytic preference for the semi-hydrogenation of acetylene to ethylene. The trend isolated appears to be universal and marks a subspace within intermetallic compounds that is promising to focus further studies upon. Results also suggest the possibility of accessing New Brønsted-Evans-Polanyi relationships over a subspace of intermetallic compounds.

© 2019 Elsevier Inc. All rights reserved.

1. Introduction

Unsaturated hydrocarbons are critical chemical building blocks in the chemicals industry, yet their production and functionalization continue to be a challenge as the chemical industry shifts from cracking large petroleum-based polyaromatics to the upgrading of small molecules to olefins and aromatics [1]. Unsaturated C-C bonds exhibit elevated reactivity, which is both the source of their value as well as the difficulties encountered in their production and functionalization. A multitude of chemical processes rely upon catalysts that preserve C=C bonds in product molecules or gently activate C=C bonds in reactants to facilitate their selective functionalization through hydroreactions, e.g., semi-hydrogenation of alkynes, linear and cyclic alkane dehydrogenation, selective hydrogenation of unsaturated aldehyde, many hydrofunctionalization reactions, biomass deoxygenation, etc. [2-13]. However, in many cases, selective and highly tunable catalysts are still lacking for current and future catalytic applications [14-20]. In an effort to expand the roadmap for new catalytic materials, we have focused upon understanding the surface and catalytic chemistry of intermetallic compound (IMC) catalysts in a systematic fashion. Specifically, Ni-based IMCs with p-elements from the boron group. This class of materials has demonstrated uniquely favorable surface and catalytic chemistry in olefins production and is naturally compositionally rich [10,21–32]. The reaction of semi-hydrogenation of acetylene has been utilized to illustrate control of surface chemistry towards two different types of unsaturated C—C bonds in a hydrogenation environment. Studies were limited to equimolar bulk stoichiometry Ni + B-group IMCs such that all materials were isoelectronic.

IMCs comprised of non-noble metals mixed with post-TMs or semimetals, where bulk bonding is strong enough to drive the formation of compositionally ordered compounds, marks a promising compositional space that may exhibit wholly new surface and catalytic chemistry due to strong electronic effects. Within the context of olefin production, results from several studies suggest IMCs that are comprised of elements of similar size appear to promote improved orbital overlap, strong bonding within the bulk, reduced surface reactivity, and improved catalytic performance in olefin production, e.g., Ni + Al, Ni + Ga, Ni + Sn, Pd + Ga, Pd + In, Co + Ge, Pt + Sn, Pd + Sn, etc. [8,10,24,26,29,30,33-40]. Additionally, bulk stoichiometry and surface compositions that are equimolar or p-element rich also roughly correlate with elevated selectivity towards olefin production and reduced oligomerization in semi-hydrogenation of alkynes [24,34-36,41,42]. An effect associated with IMC constituent element electronegativity manipulating the Fermi level energy and surface chemistry of the IMC is

^{*} Corresponding author.

E-mail address: slaursen@utk.edu (S. Laursen).

also evident, but has yet to be clearly established [22,43–45]. Nonetheless, understanding what produces and controls the favorable surface chemistry of IMCs is of significant interest.

A selection of experimental and computational studies have already suggested that reduced surface reactivity and limited hydrogenation activity are the source of the special catalytic activity of these IMCs. Experimental studies have shown that olefins, aromatics, and CO all bind less strongly over IMCs in comparison to their parent metals [21,29,31,38,46]. This less aggressive surface reactivity correlates well with improved selectivity in olefins/aromatics production [10,24-27,32]. Indeed, improved control or limited hydrogenation has been connected to inhibited atomic H transfer as tracked by markedly reduced H₂/D₂ isotope scrambling [29,30]. Despite a lack of reaction site composition characterization in experimental studies, computational surface science studies have demonstrated that the p-element plays a crucial role in modifying the surface and catalytic chemistry of IMCs [22.47–52]. Specifically, that limited hydrogenation activity and reduced surface reactivity towards C=C bonds are connected to p-element contributions to the surface chemistry [22,34,47,50-55]. Strong electronic effects that greatly modify the reactivity of both TM and p-element in IMC surface chemistry have also been reported as well as the formation of bulk electronic structures markedly different from the constituent elements [36,41,45].

Despite generally good agreement between experiment and computational surface science studies thus far, several challenges are still present in the study of IMC catalysts regardless of approach. Computationally, many basic aspects of modeling IMC surfaces must be determined on a case-by-case basis and/or inferred from heuristics. Of critical concern is IMC surface facet composition/termination, which cannot currently be treated with ab initio thermodynamics approaches due to a lack of p-element source reference that is both computationally convenient and experimentally realizable [55-58]. In the Density-Functional Theory (DFT) approach, the most appropriate exchange-correlation functional for calculating IMCs has also yet to be determined. Because the bonding within IMCs may depart significantly from that found in monometallic TM or TM + TM alloy solids, newer functionals focused on capturing more localized bonding or highly hybridized electronic structures may be needed [59–65].

Experimentally, study of IMCs is equally challenging due to a lack of synthesis techniques that produce high surface area nanoparticles in phase-pure form with specific surface compositions. The degree at which element segregation occurs at the IMC particle surface is also not well established and is likely dependent upon individual IMC compositions and reaction condition features [66–70]. The quality of IMC surface composition characterization is also lacking with many investigators utilizing techniques that yield information from the topmost several nanometers of the material rather than the outermost few atomic layers, e.g., XPS, EDS line scans, etc. [24,29,30,35–39,41]. Studies that utilize more appropriate techniques such as TOF-SIMS or HS-LEIS becoming more common, yet are still fairly scarce compared to the number of possible IMCs [42,58,73,71,72,74-76]. Noting these issues is critical such that the source of any lack of correlation between experimental and computational studies may be isolated and eventually corrected.

To begin to systematically understand the effect of p-block element selection on the surface and catalytic chemistry of IMCs in the production of olefins, we have performed an exhaustive computational surface science study over Ni + B-group IMCs (NiB, NiAl, NiGa, NiIn, and NiTl) in the context of the semi-hydrogenation of acetylene. Several aspects dictated the reaction and materials selection. To simplify the reaction system to one that was dependent only upon the surface chemistry towards carbon and hydrogen, acetylene semi-hydrogenation was a natural choice. The

reaction allowed for the investigation of the hydrogenation of two unsaturated C-C bonds of differing reactivity. The Ni + B-group IMCs of 1:1 bulk stoichiometry were chosen for several reasons: (i) the existence of experimental studies in the semi-hydrogenation of acetylene, (ii) simple bulk crystal structures, and (iii) easily identified surface facets and terminations. The Ni + B-group IMCs are also isoelectronic at the 1:1 stoichiometry. This allowed for the effect of orbital overlap between Ni and the p-element in dictating the nature of bulk bonding and surface and catalytic chemistry to be investigated. Four XC functionals were utilized for the Density Functional Theory (DFT) calculations to facilitate comparison and to determine where functional choice may be more sensitive with respect to IMC composition. In addition to PBE-sol, PBE, RPBE, and PW91 were utilized to understand if new non-metallic-solids-focused functionals (PBE-sol) are necessary to capture the surface chemistry of IMCs [59.62.77–80].

2. Methods

Density-Functional Theory (DFT) quantum chemical modeling calculations were performed using the Vienna Ab Initio Simulation Package (VASP 5.3.5) and resources from Extreme Science and Engineering Discovery Environment (XSEDE) [81–85]. Hydrogen was modeled with an ultra-soft pseudopotential and larger atomic cores were modeled with Projector Augmented-Wave (PAW) potentials. Calculations were performed with the generalized gradient approximation (GGA) of PBE-sol exchange-correlation functional which is a modified version of PBE [62,86]. In comparison to PBE, PBE-sol is tuned to lessen the dependency on the electron density gradient in the functional. This modification can reduce the nonlocality of GGA PBE such that more covalent bonding characteristics within solids can be captured even if there is no band gap present. PBE-sol has been shown to significantly improve the calculation of surface energy, lattice parameters, surface exchange and correlation, and energy for materials that contain covalent bonds within solids. Therefore, the use of PBE-sol may be necessary to properly capture the bonding within IMCs and more appropriately capture IMC surface chemistry [59,62,77-80,86-88]. To investigate the effect of XC functional choice, calculations were also performed with PBE, RPBE, and PW91 (minor changes were found, see Table S12 in the Supporting Information).

All calculations were performed using a plane wave basis with an electronic plane wave cut-off of 400 eV. The vacuum space between repeated slabs was set to up to 25 Å to eliminate the interaction between slabs. For all calculations, the two topmost atomic layers of slab models and adsorbates were allowed to relax and optimize, and the rest of layers were fixed at DFT-optimized bulk positions. To efficiently sample the first Brillouin zone, different k-points grids were chosen depending upon areal slab size. The first Brillouin zone was modeled with gamma centered grid of high k-point $(5 \times 5 \times 1)$ for hydrogen dissociative adsorption using a smaller slab and k-point $(2 \times 2 \times 1)$ for other calculations that utilized a larger slab. For adsorption and surface energetics calculations, the slabs of 2 \times 2, 2 \times 2, 3 \times 3, 3 \times 3, 2 \times 2, and 2 \times 2 were utilized for Ni, NiB, NiAl, NiGa, NiIn, and NiTl, respectively. The choice of surface unit cell size for each IMC depended on the size of adsorbates. Slabs were chosen such that adsorption resulted in an approximate surface coverage of 1/4 monolayer such that lateral adsorbate-adsorbate interaction could be minimized. The climbing nudged elastic band (cNEB) and DIMER method were utilized to isolate and confirm transition states [89–92]. The effect of model size, k-point sampling, and cut-off energy on observed surface chemistry was checked and the values stated above yielded a reasonable balance of accuracy and computational efficiency. For

all reported energies, positive values indicate endothermic energetics and negative values indicate exothermic energetics.

Hydrogen dissociative adsorption energy was used as a marker for the surface reactivity towards atomic hydrogen. Acetylene and ethylene adsorption and distortion energies were chosen as markers to predict surface reactivity towards carbon. The adsorption energies were calculated with Eq. (1) using gas phase molecular references.

$$\Delta E_{ads} = E_{total} - E_{slab} - E_{gas} \tag{1} \label{eq:delta-E}$$

For energetics within the reaction mechanism where stable gas phase molecular species are not available to use as a reference, changes in energy between initial and final state were used.

The distortion energy was defined as the energy difference between a gas phase molecule and the molecule in the geometry induced through adsorption in the absence of the catalyst surface. Distortion energy may provide additional insights into the nature of the changes brought about by adsorption and aid in deconvoluting adsorption energies that include contributions from both the adsorbate and changes in the catalyst surface.

Magnetic properties of Ni and Ni + B-group IMCs were calculated to properly capture their electronic structure and surface chemistry. Nickel in the monometallic Ni(111) surface was calculated with an optimized magnetic moment of 0.63 μ_B [93,94]. Ni + B-group IMCs all exhibited no magnetic moments under any circumstances, which agrees with literature results [95–98].

All materials were modeled using the lowest energy facets as determined from literature or manually through as-cut surfaces. Surface termination was not adjusted for reaction conditions. The model slabs contained at least four atomic layers. The most favorable surface facets of NiAl(110) [99,100] and NiGa(110) [26] have already been established in previously published studies by others. When surface facets were determined manually, the candidate surface facets were those with the maximum surface ion packing symmetry and minimum surface ion-ion interaction and corrugation. The surface composition of the slabs was not modified beyond the as-cut compositions. The simplicity of the 1:1 bulk stoichiometry crystal structures allowed for reasonable surfaces to be selected and their surface energies calculated. The surface energies of the candidate facets were compared and the lowest energy facets were utilized as the most favorable facets. Surface energies of different facets for each material are presented in Fig. S1. Using this approach, the facets of NiB(001), NiAl(110), NiGa(110), NiIn(001) and NiTl(110) were manually identified as the most favorable surface facets. Because IMCs are produced through a melting process or via reduced salts on a support surface, there are no appropriate references for source elements for an ab initio thermodynamics approach. Therefore, surface terminations were dictated simply by the cut of the crystal in its as-cut composition. The super-cell size of slab models was 2×2 or 3×3 multiples of the most basic surface symmetry unit cell. It is important to note that these super cells are significantly larger than those of the same designation for close-packed pure metal surfaces.

The Gibb's free energy of the surface reaction mechanism for semi-hydrogenation of acetylene over each surface were calculated under common reaction condition (425 K, 1 atmosphere with 5% acetylene, 0.5% $\rm H_2$, and 49.5% ethylene). Gibb's free energy was calculated as Eq. (2).

$$G = E + E_{vib} + PV - TS \tag{2}$$

where G is Gibb's free energy, E and E_{vib} are internal energy and vibrational energy of the systems. Internal energy, E, is from DFT calculation. The order of magnitude of PV term contribution is very small, which can be treated as zero. The effect of entropy change was considered only for the adsorption and desorption steps since entropy changes of surface reactions are minor contributors

[101–103]. The entropic contributions to adsorption and desorption as a function of temperature and pressure was obtained from NIST thermochemical tables [104].

To isolate the active reaction pathways and rate determining steps within the active mechanisms, microkinetic modeling was utilized to calculate the rate constants and activity of rate-determining steps for different reaction pathways. The reaction conditions were set to 425 K, 1 atmosphere with 5% acetylene, 0.5% H₂, and 49.5% ethylene. The rate constant is given by Eq. (3) [105]:

$$k = \frac{k_B T}{h} \frac{Q_{TS,vib}}{Q_{IS,vib}} e^{\frac{-E_a}{k_B T}}$$

$$\tag{3}$$

where k_B is the Boltzmann constant, T is the absolute temperature, h is the Plank's constant, $Q_{TS,vib}$ and $Q_{IS,vib}$ are the partition functions for the transition state and the initial state, respectively, and E_a is the activation energy calculated from DFT. Q_{vib} is calculated as:

$$Q_{vib} = \prod_{i} \frac{1}{1 - e^{\frac{-hv_{i}}{k_{B}T}}} \tag{4}$$

where v_i is the vibrational frequency of each vibrational mode of the adsorbates computed from DFT calculations.

3. Results

As an outline, the study consisted of determining the energetics for all reasonable pathways including the selective hydrogenation of acetylene to ethylene, unselective overhydrogenation of ethylene to ethane, oligomerization through C—C coupling of the intermediates HCCH + HCCH₂, and coke formation through acetylene C-C cleavage before and after dehydrogenation. While determining the mechanism, an exhaustive search was performed to find the most energetically favorable reaction site for each reaction step over each material. Kinetic rate constants were then calculated using DFT-determined activation barriers and pre-exponential factors and used to isolate rate-determining steps and dominant reaction pathways for each material. Van der Waals interactions were not included in the calculations. A minor substudy of the effect of atomic H surface coverage was also performed for selected materials, but was limited to thermodynamics at this point. This effect will be fully studied using kinetic Monte Carlo simulations in the future. Relative rates were utilized in a Sabatier analysis to correlate with surface reactivity markers such as adsorption and molecular distortion energy of acetylene and ethylene and dissociative H₂ adsorption. Due to the availability of three distinct reaction pathways in the reaction network, the Sabatier analysis was limited to individual pathways for clarity. In-depth electronic structure analysis using band structure, density of states, and Bader charge analysis was performed to correlate with calculated surface and catalytic chemistry and surface reaction site preference and composition. For bulk IMC crystal structure details see the supplemental document.

3.1. Description of surfaces

First, a description of the surfaces of the 1:1 bulk stoichiometry Ni + B-group IMCs used in the study to clarify the nature of the surface reaction sites present. The highest symmetry, close-packed surfaces with as little surface corrugation and like-element interaction were considered and their surface energies compared (see Fig. S1). The surfaces used for the reaction analysis exhibited the highest surface packing symmetry and lowest energy. Because of the simplicity and symmetry of the bulk crystal structures, facet cuts were symmetric in the z-direction enabling unconvoluted surface energy calculations. In addition, the composition of the

surfaces was determined by as-cut bulk stoichiometry and not modified further (see methods and Fig. S1). The most favorable facets for Ni + B-group IMCs were NiB(001), NiAl(110), NiGa(110), NiIn(001) and NiTl(110) with the lowest surface energy. All surfaces besides NiTl exhibited in-plane close-packing of elements of the highest degree possible with no surface corrugation. As-cut surfaces were utilized for all surfaces, thus their termination/composition was naturally dictated by the bulk stoichiometry of the crystals. The element packing of all surfaces besides NiIn showed rows of Ni atoms separated by p-elements, which provided Ni-Ni bridge, mixed composition three and fourfold hollows, bridge sites consisting of two p-elements, and atop reaction site possibilities.

The possible reaction sites for Ni + B-group IMCs are shown in Fig. S4. Over the NiB(001) surface, one Ni atom was surrounded with three B atoms. Six types of reaction sites were present including a Ni atop site (A1), a B atop site (A2), a Ni-Ni bridge site (B1), a B-B bridge site (B2), a Ni-B bridge site (B3), a threefold hollow of 2Ni and B (T1), a threefold hollow of Ni and 2B site (T2), and a fourfold hollow site of 2Ni and 2B (H1). NiAl(110) and NiGa(110) exhibited the same surface atom packing that contained one Ni atom surrounded by four Al or Ga atoms. The possible reaction sites over NiAl(110) and NiGa(110) surfaces were a Ni atop site (A1), an Al or Ga atop site (A2), a Ni-Ni bridge (B1), a Al-Al (or Ga-Ga) bridge (B2), a Ni-Al bridge site (or Ni-Ga bridge site) (B3), a threefold hollow of 2Ni and Al (or 2Ni and Ga) (T1), a threefold hollow of Ni and 2Al (or Ni and 2 Ga) (T2), and two hollow sites of 2Ni and 2Al (or 2 Ga) (H1 and H2). NiIn(001) is unique in that it presents an additional Ni-dominated threefold hollow site. NiIn(001) presented a threefold Ni ensemble as well as a Ni atop site (A1), an In atop site (A2), a Ni-In bridge site (B1), a threefold hollow of 3Ni (T1), a threefold hollow of 2Ni and In (T2), and a fourfold hollow of 3Ni and In (H1). The lowest energy surface of NiTl(110) exhibited some free space thus tests were performed by adding Ni or Tl to the surface to determine if alternate surface terminations were stable and/or presented markedly different reactivity (see Fig. S3). Added Tl was expelled from the surface and added Ni lead to very similar surface reactivity in adsorption probes as the as-cut surface. Therefore, in the limit of this study, the as-cut NiTl surface was used throughout thestudy. The NiTI(110) presents a Ni atop site (A1), a Tl atop site (A2), a Ni-Ni bridge site (B1), a Ni-Tl bridge site (B2), a threefold hollow site of 2Ni and Tl (T1), and a threefold hollow site of 3Tl (T2). In the vernacular of physical TM ensembles, all surfaces besides NiIn present twofold Ni ensembles.

3.2. Nature of reaction sites for adsorbates and intermediates

Summarizing where adsorbates and intermediates preferentially adsorb and the composition of the reaction sites over each surface before presenting the kinetic analysis helps to illustrate how changes in the electronic structure of the materials promotes differences in the relative contributions of Ni and the p-elements to the surface and catalytic chemistry. In general, where the pelement size starts to match that of Ni, as in NiAl and NiGa, strong electronic effects begin to be evident. Once the p-element is larger than Ni and reduced orbital-orbital overlap effects are present, ensemble type Ni-dominated surface chemistry is more prevalent. The covalent element sizes of Ni and B-group p-block elements as determined through bonding with C are stated next to the model surface pictures in Fig. 1a [106]. The radii track as B < Ni, Al and Ga similar to Ni, and In and Tl > Ni. The relative element sizes were used to approximate the orbital overlap between Ni and the p-elements, and was found to track well with IMC surface and catalytic chemistry. The effect of orbital overlap between Ni and

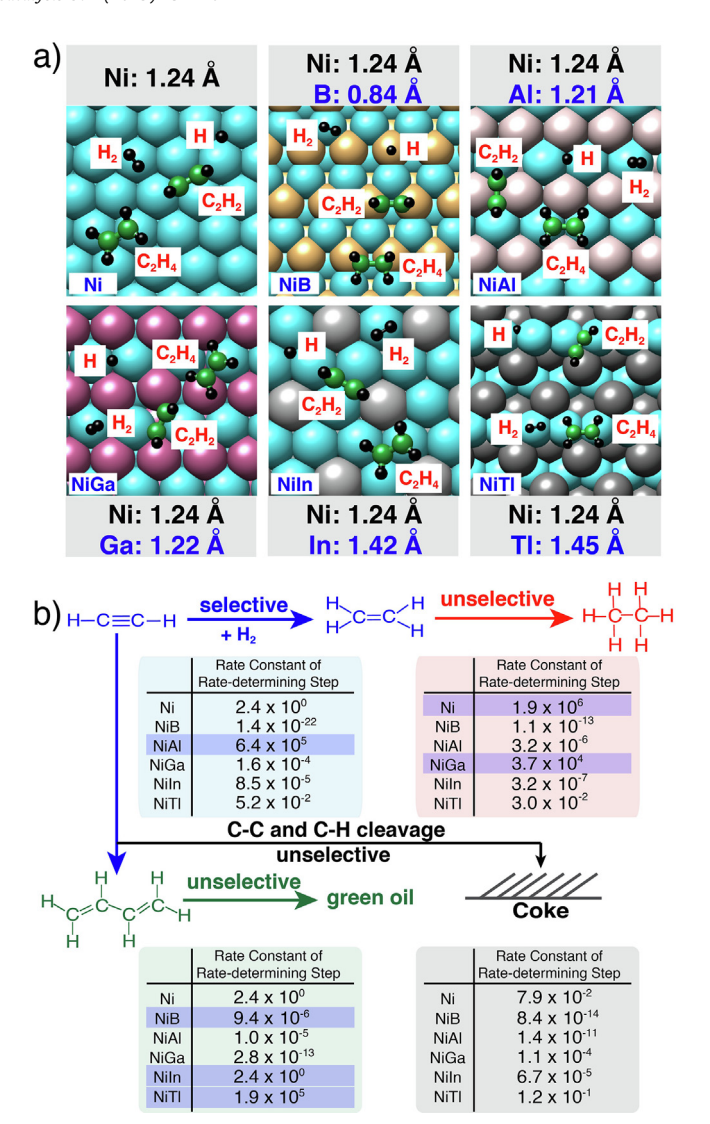


Fig. 1. (a) illustrative model surfaces with acetylene, ethylene, molecular H₂, and atomic H adsorbed over Ni and Ni + B-group IMCs; (b) Rate constants for each reaction pathway in semi-hydrogenation of acetylene. Elements in the model figures are color coded: Ni (light blue), B (yellow), Al (light gray), Ga (magenta), In (medium gray), Tl (dark gray), C (green) and H (black).

p-block element on electronic structure and surface and catalytic chemistry will be discussed later.

The most favorable adsorption sites for acetylene, ethylene, molecular H₂, and atomic H over Ni and Ni + B-group IMCs are presented in Fig. 1a. The most favorable reaction site for molecule H₂ over all surface was atop a Ni site. In the case of NiB, the most favorable reaction sites for acetylene, ethylene, and atomic H were a B-B bridge site (B2), hollow site (H1) that consisted of 2Ni and 2B. and atop B site (A2), respectively. In the case of NiAl, acetylene preferentially adsorbed on the hollow site (H1) that consists of 2Ni and 2Al atoms. The most favorable reaction site for ethylene and atomic H were a Ni-Ni bridge (B1) and a hollow site of (H2) that consisted of 2Ni and 2Al atoms, respectively. The two hollow sites are compositionally distinct due to the geometry being different. Similarly, in the case of NiGa, the most favorable adsorption site for acetylene and atomic H was also a hollow site (H2) that consists of 2Ni and 2 Ga atoms. However, ethylene adsorbed preferentially at a Ni-Ga bridge site (B3). Over NiIn, the most favorable reaction site for acetylene, ethylene, and atomic H were the threefold hollow site of 3Ni (T1). Over NiTl, acetylene was preferentially

adsorbed over the threefold hollow site of 2Ni and Tl (T1). On the other hand, the most favorable ethylene and atomic H adsorption sites were Ni-Ni bridge (B1).

The reaction pathways of acetylene hydrogenation include selective hydrogenation of acetylene to ethylene, overhydrogenation of ethylene to ethane, oligomerization of acetylene to butadiene, and C-C and C-H cleavage of acetylene (see Fig. 1b). The nature and composition of each surface reaction site for all intermediates calculated are summarized in the Tables S5, S6, and S7. Because atomic H can move to a meta-stable site directly before hydrogenation events, the composition of the meta-stable site was also highlighted (see Table S9). We find that NiB, NiAl, and NiGa exhibit electronic effects that promote mixed Ni and pelement composition reaction sites in almost all reaction steps throughout the reaction network. NiB stands apart in that most reaction steps occur over the B-B bridge or at an atop B site with no direct Ni contribution, e.g., for C_xH_y intermediates and H. Only two instances deviated from this trend: ethylene adsorption at the H1 hollow site of 2Ni and 2B and CH adsorption (after C-C cleavage of acetylene) favored the T1 site of 2Ni and B. Over NiAl and NiGa, 18 of 24 reaction steps over NiAl and 23 of 24 reaction steps over NiGa occurred at mixed composition reaction sites such as T1, T2, H1, and H2 sites. The exceptions were: for NiAl, the 1st and 2nd hydrogenation of ethylene to ethane and the hydrogenation of C₄H₅ to C₄H₆ that occur atop a Ni site; for NiGa, the 2nd hydrogenation step of ethylene to ethane favored Ni atop site. Interestingly, the nature of metastable site of atomic H before hydrogenation over NiB, NiAl, and NiGa was also dominated by either mixed composition or only the p-element. The situation is opposite over NiIn and NiTl where most reactions occur at Nionly bridge or hollow sites. Notably, 23 of 24 reaction steps over NiIn occur at Ni-dominated sites. The only exception was CCH (after acetylene dehydrogenation) favored the H1 site of 3Ni and In. Reaction sites over NiTl were wholly dominated by Ni with no Tl contribution. More details for the individual reaction sites can be derived from Tables S5, S6, S7, and S9.

These trends already show the effect of orbital overlap with three distinct reaction site composition cases. Results also contrast considerably with established understanding of the surface chemistry of PGM alloys and PGM IMCs where reaction sites are dominated by TMs and ensemble or ligand effects are commonly observed [21,36,41,45,107–112]. Results suggest that when a more reactive TM is used in TM + p-element IMC compositions, more significant reorganization of the TM electronic structure occurs and p-states from the p-element are within range of the Fermi level such that they can participate in the surface chemistry. This effect has the potential to bring about wholly new surface chemistry for both the TM and p-elements at the surface as well as in their combined composition hollow or bridge sites. This assertion is supported by our electronic structure analysis presented later.

3.3. Kinetic analysis of reaction pathways

A kinetic rate analysis was performed to understand the kinetic preference for each catalyst for the selective production of ethylene, unselective overhydrogenation to ethane, oligomerization via HCCH + HCCH₂ coupling, and coke formation via C—C cleavage before or after acetylene is dehydrogenated (see Fig. 1b). Acetylene hydrogenation is necessary to initiate all reaction pathways besides those associated with coking; therefore, it may kinetically limit both production of ethane and butadiene in the oligomer pathway. As a basis, Ni is predicted to exhibit both ethane production and oligomerization activity. Over the Ni + B-group IMCs, results indicate that only NiAl would exhibit high selectivity towards ethylene production with limited oligomerization. NiB is

predicted to be mostly catalytically inactive due to aggressive surface reactivity. NiGa, with the hydrogenation rate of ethylene to ethane several orders of magnitude higher than acetylene hydrogenation, would suggest all ethylene would be converted to ethane but be kinetically limited by acetylene hydrogenation. The relative rates for ethylene and ethane production over NiIn indicate it may show some selectivity towards ethylene, but because the oligomerization rate over this surface is substantial, oligomerization is likely preferred. A similar case is encountered over NiTl with acetylene hydrogenation preferentially branching to oligomerization rather than ethane production. Oligomerization over NiAl or NiGa appear to be relatively limited. In the pathway to coke formation, assumed to be associated with acetylene C—C cleavage before or after its dehydrogenation, only Ni and NiTl exhibit rates that are comparable with other pathways.

In addition, the effect of coverage of H on the reaction energetics was investigated to a limited extent. As this is a study in and of itself that requires appropriate simulation techniques, the effect of H coverage was limited to the thermodynamics of acetylene hydrogenation to ethylene over NiAl, NiGa, and NiIn (see Figs. S10, S11, S12). A simulation study using kinetic Monte Carlo will be published in a follow-up study. The results showed 0.3 eV maximal change of thermodynamics of hydrogenation over these three materials but with different trends. Over NiAl, the 1st hydrogenation of acetylene actually became less favorable (ΔE changed from -0.2 eV to -0.1 eV) when the H coverage increased from 0.2 to 1. Whereas, the 2^{nd} hydrogenation of acetylene became less favorable (ΔE changed from 0.0 eV to +0.1 eV) when H coverage increased from 0.2 to 0.6 and then became more favorable (ΔE changed from +0.1 eV to -0.1 eV) when H coverage increased further to 1.0. Over NiGa, the 1^{st} hydrogenation of acetylene became less favorable (ΔE changed from -0.3 eV to -0.2 eV) when the H coverage increased from 0.2 to 1.0. The 2nd hydrogenation of acetylene over NiGa became less favorable with ΔE changed from 0.0 eV to +0.3 eV when the H coverage increased from 0.2 to 0.4, and then became more favorable with ΔE changed from +0.3 eV to 0.0 eV when H coverage increased further to 1.0. The NiIn case showed an opposite trend where both 1^{st} and 2^{nd} hydrogenation of acetylene became slightly more favorable when the H coverage increased (ΔE changed from +0.9 eV to +0.8 eV for the 1st hydrogenation step and remained the same for the 2^{nd} hydrogenation step). These trends contrast with the phenomenon observed over metal surfaces where high coverage of H promotes hydrogenation [113-115]. The contribution of the p-element to the IMC electronic structures clearly modifies this basic surface chemistry effect and must be understood through further studies.

Comparing to experiments illustrates the role of inexactness in IMC synthesis, most notably with respect to the surface composition of the IMC catalysts, which is an ongoing challenge [25,28,30,31,37,38,116]. Because the synthesis of IMCs with bulk-like stoichiometric surface compositions is not well established nor is it common to characterize the IMC surface composition with sufficiently surface-sensitive techniques, many studies suffer from IMC catalysts with nonideal surface terminations [10,21,24,26,27,29,30,38,39]. These issues convolute comparison with computation, but once accounted for, some agreement can be isolated.

For example, Raney nickel (NiAl) has been shown to exhibit low selectivity towards ethylene in the semihydrogenation of acetylene and appreciable C=C hydrogenation in selective hydrogenation reactions [10,116–120]. However, this disagreement is likely due to Ni-rich surfaces produced through the oxidation of Al and its removal when "activating" the material through etching procedures [118,120–122]. Therefore, careful oxygen-free synthesis and storage of NiAl would be required to produce the activity predicted herein. Experimental observations for Ni and NiGa in the

semi-hydrogenation of alkynes agrees well with our calculations that show high rates for C=C hydrogenation [2,24,26,123]. In the case of NiIn for semi-hydrogenation, experimental results are limited to a study that utilized various Ni and In nominal loadings on SiO₂ [27]. It is noted that XRD of the materials showed mixed phases throughout. Nonetheless, the NiIn/SiO₂ catalyst exhibited high selectivity (60%) towards oligomerization, which agrees with our predictions. Studies using Ni + In IMCs in selective hydrogenation further showed that C=C bonds were preferentially hydrogenated [37]. No experimental studies of NiTl in catalysis are currently available.

Comparing to experimental studies of NiB_x compounds, none have been used in acetylene semi-hydrogenation, but the selective hydrogenation of the C=C bond within unsaturated aldehydes has been demonstrated [124–127]. This activity contrasts with our calculations only because we focused upon the lowest energy reaction pathway and its reaction sites. The less reactive Ni-rich or Ni-only sites present at the Ni boride surface may contribute significantly to the more facile hydrogenation observed experimentally (see Tables S3 and S4 for acetylene and ethylene adsorption at B and Ni sites over NiB). Additionally, increasing the B concentration in the NiB_x has been shown to drive even more C=C hydrogenation but result in severe deactivation [123,128,129]. Comparing with IMCs produced from a PGM such as Pd supports the presence of a systematic trend in the effect of element size in the IMC. Considering that Pd is larger, the p-elements that would produce similar low surface reactivity would need to increase in comparison to the Ni IMCs. For example, the special surface chemistry is observed for PdGa and PdIn illustrated by improved selectivity towards ethylene and inhibited oligomerization in the semi-hydrogenation of acetylene [34-36,41]. The same size-match effect is evident in our study of NiAl and NiGa. This trend was also demonstrated in other IMC compositions where element sizes match, e.g., PdGa, PdAg, and PtSn in selective hydrogenation, dehydrogenation, and deoxygenation reactions and in computational studies [2,36,47,130-131].

3.4. Sabatier correlation analysis

Sabatier correlations between activity and surface chemical reactivity markers were investigated to shed light upon the contributions of different surface chemistries to the calculated relative rates. Significant changes in surface chemical reactivity of the suite of IMCs towards intermediates and reactants as a function of pblock element produces an equally significant range of relative activities in each reaction pathway (see Fig. 2a, b, and c). Sabatier correlations for hydrogenation of acetylene to ethylene, hydrogenation of ethylene to ethane, and oligomerization of acetylene to butadiene are shown in Fig. 2a, b, and c, respectively. The x and y- axis are the surface chemical reactivity markers acetylene or ethylene adsorption energy, and H₂ dissociative adsorption energy. The z- axis is the relative activity calculated as a normalized kinetic rate constant ($log(k/k_{max})$). Correlations were produced for individual reaction pathways due to the lack of a common surface reactivity marker that dictated activity in all three pathways. Significant sampling of each correlation space by the suite of materials indicates no one surface reactivity marker is able to describe the relative activity of the materials. General observations locate the maximum in activity for acetylene hydrogenation around $\Delta E_{diss.ads,H_2}$ of -0.5 eV and $\Delta E_{ads,C_2H_2}$ of -2.3 eV (shown in Fig. 2a). Likewise, in ethylene hydrogenation, the maximum is predicted around $\Delta E_{\textit{diss.ads},H_2}$ of -0.5 eV and $\Delta E_{\textit{ads},C_2H_4}$ of -1.0 eV, which is in line with the established understanding of lower surface reactivity towards hydrogen and moderate binding of the molecule to be hydrogenated leads to more rapid hydrogenation (shown in

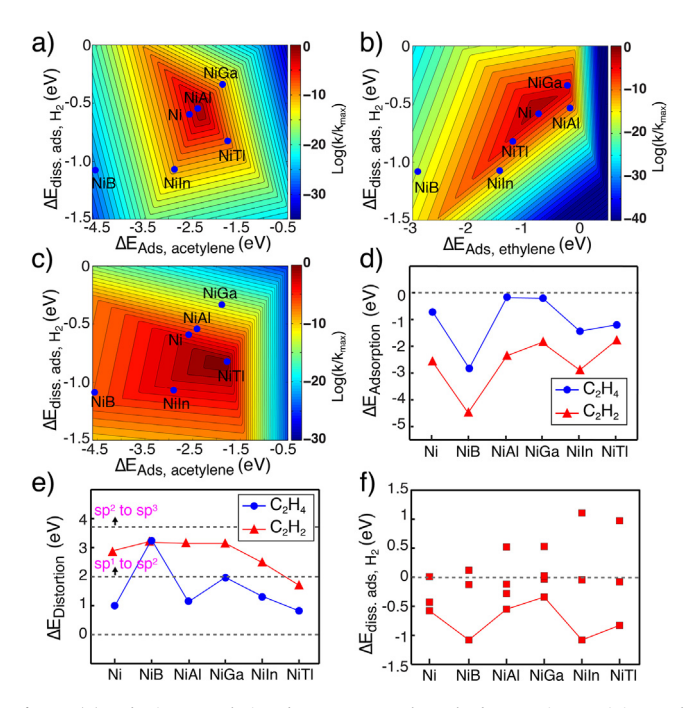


Fig. 2. (a) Sabatier correlation between acetylene hydrogenation activity and acetylene adsorption and H₂ dissociative adsorption; (b) Sabatier correlation between ethylene hydrogenation activity and ethylene adsorption and H₂ dissociative adsorption; (c) Sabatier correlation between oligomerization activity and acetylene adsorption and H₂ dissociative adsorption; (d) acetylene and ethylene adsorption energy over Ni and Ni+B-group IMCs; e) acetylene and ethylene distortion energy over Ni and Ni+B-group IMCs; (f) H₂ dissociative adsorption energy over Ni and Ni+B-group IMCs on different adsorption sites, points connected by line are on the most favorable sites, and others not connected by line are on the less favorable sites.

Fig. 2b). The maximum in activity for the production of the oligomer precursor butadiene resides at $\Delta E_{diss.ads,H_2}$ of -0.8 eV and $\Delta E_{ads,C_2H_2}$ of -1.8 eV (shown in Fig. 2c). The lack of systematic and localized linear trends that were a function of only one surface chemical reactivity marker, as commonly encountered over monometallic surfaces, further suggests significant ensemble or electronic effects in the Ni + B-group IMC surface and catalytic chemistry [2,21,110,132–134]. As all Ni + B-group IMCs are isoelectronic, the changes in surface chemistry are driven predominantly by changes in orbital-orbital overlap, electronegativity differences between Ni and the p-element, and a minor ensemble effect (threefold to twofold Ni reaction sites, where applicable).

4. Discussion

4.1. Deviations from established metal-derived BEP relationships

In developing structure-activity relationships for the Ni + B-group IMCs, the nonmonotonic changes within the electronic structure and surface chemistry as a function of p-element selection must be accounted. Correlating kinetics with individual surface chemical reactivity markers, thermodynamics for reaction steps, or d-band centers over all materials show a rough general linear trend, but significant deviations are found for the IMCs that exhibit stronger electronic effects and p-element contributions to reaction sites, e.g., over NiB, NiAl, and NiGa (see Figs. S13, S14, S15, S16, and S17). Specifically, the deviations in correlation between ΔE and E_a indicate that new BEP correlations may be accessed over IMCs despite the limited materials studied herein.

Considering adsorption probes as surface reactivity makers, general changes in surface reactivity as a function of p-block

element agrees roughly with observed reaction pathway preference, but some critical deviations are present over NiAl and NiGa. Acetylene, ethylene, and dissociative H₂ adsorption follow a rough volcano-like trend with NiAl and NiGa exhibiting the lowest reactivity towards the adsorbates (see Fig. 2d, e, and f). The reduced surface reactivity of NiAl and NiGa correlate well with improved orbital overlap where the element sizes match. Whereas, for smaller (B) or larger (In or Tl) p-block elements where a size mismatch occurs with Ni, greatly elevated surface reactivity is encountered. It is first noted that all surfaces readily dissociate H₂ (E_a ranged from 0.0 to +0.3 eV) (see Table S8). Therefore, the availability of atomic H is not likely a controlling factor in the predicted catalyst performances. The aggressive nature of B-dominated reaction sites of NiB correlates well with high barriers throughout the reactions on its surface. Weaker vet still significant adsorption of acetylene and ethylene over Ni-dominated sites of NiIn and NiTl correlates well with C—C coupling, vet hydrogenation is limited. The reduced binding of key hydrocarbon and intermediates adsorbates over NiAl and NiGa would naturally suggest more facile complete hydrogenation to ethane and more facile C-C coupling, yet this is not observed in the reaction energetics analysis further indicating a departure from metal-derived BEP correlations. The energetics of hydrogen transfer from the surface to the intermediate appear to drive these differences. For example, acetylene hydrogenation is an order of magnitude faster than ethylene hydrogenation over NiAl and the opposite over NiGa.

Focusing on correlations between thermodynamic driving forces and kinetic barriers, similar deviations from metal-derived BEP correlations (Ni specifically) are encountered for NiB, NiAl, and NiGa (see Figs. S7 and S8). In acetylene hydrogenation, the 1st hydrogenation over NiB and both 1st and 2nd hydrogenations over NiGa deviate with higher barriers than expected with respect to their thermodynamic driving forces. In ethylene hydrogenation, both hydrogenations over NiB and NiAl and the 2nd hydrogenation over NiGa deviate similarly with higher barriers than expected from the general metal-derived BEP correlation. Again, these deviations occur over the three materials that exhibit the greatest electronic structure changes upon IMC formation or significant/dominant contributions from the p-element in the surface reactions. These trends are most evident in comparing Ni, NiAl, and NiGa, as presented in Fig. 3. Within acetylene hydrogenation, the greatly elevated reactivity of acetylene likely played a role in normalizing hydrogenation BEP correlations due to it circumventing changes in surface reactivity driven by changing the p-element in the IMC. These results suggest that scrutinizing simple reactivity markers is insufficient to understand the surface and catalytic chemistry of the IMCs. Instead, the electronic nature of the bonding of critical surface species and the role of IMC electronic structure in dictating surface chemistry must be scrutinized in detail to understand the predicted surface and catalytic chemistry as a function of p-element selection. Similar indications of new BEP correlations have been isolated in the study of other IMCs such as PdIn, PdGa, Al₁₃Fe₄, Al₁₃Co₄, Al₅Co₂, and Ni₃Ga [23,34-36,41,45,47-51,68,135,136] and in our prior studies of the surface and catalytic chemistry of Ni and Ti ceramics [43,44].

4.2. Analysis of electronic structures

Electronic analysis of the Ni + B-group IMCs beyond a focus on d-band center was found to be necessary to understand the marked changes in their surface chemistry. The critical features of the electronic structure of the IMCs are: (i) the degree of hybridization of the d- and p-states as indicated by band spread in the energy spectrum, (ii) the density of d- and p-states near the Fermi level that may participate in the surface chemistry, (iii) the density of non-bonding-like d-states and their proximity to the Fermi level, and (iv) the location of the Fermi level dictated

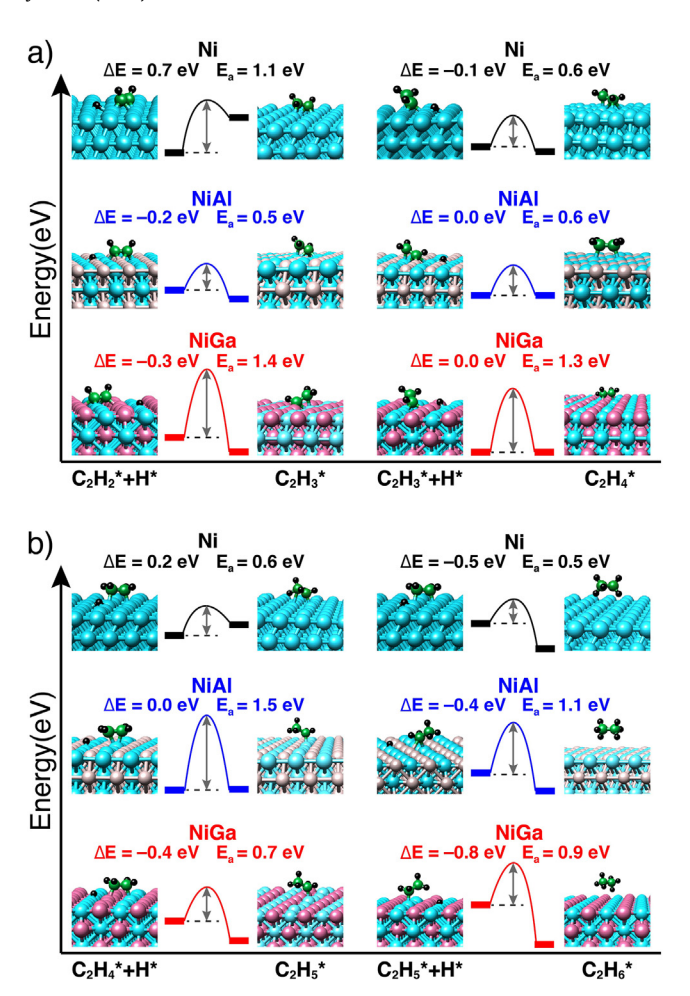


Fig. 3. Comparison of thermodynamic driving forces and kinetic barriers over Ni, NiAl, and NiGa. (a) in the hydrogenation of acetylene (b) and hydrogenation of ethylene. Elements in the model figures are color coded: Ni (light blue), Al (light gray), Ga (magenta), C (green) and H (black).

by the effective electronegativity of the IMC as modified by the p-element (see Fig. 4). The distribution of d-orbital of Ni and sand p- orbitals of p-block elements in the band structure and band spreading in energy may be used to approximate the degree of hybridization in the IMC solids (see Fig. 4, all bands plotted on a similar energy scale). Within this framework, NiB exhibited selective hybridization of d- and p-states and less energetically dispersed p-states near the Fermi level that significantly promoted B reactivity. NiAl and NiGa exhibited highly hybridized bulk bonding with significantly energetically dispersed d- and p-states. The presence of both d- and p-states near the Fermi level also promoted both Ni and Al or Ga surface site reactivity. NiIn exhibited selective hybridization between the d- and p-states and less pronounced band spreading. The nature of this hybridization promoted Ni surface reactivity. NiTl showed even less hybridization and Ni states near to the Fermi level. Again, unhybridized dstates in NiTl promote the reactivity of surface Ni sites. In general, the electronic features highlighted here correlated well with the composition of the more reactive sites over the IMCs. Results also are similar to those obtained in the electronic analysis by others of IMCs comprised of similarly sized TM and p-elements, e.g., PdGa, PdIn, FeAl, CoAl, and NiAl [36,41,45,97,137,138]. Several also noting more covalent bonding leading to lower surface reactivity. It should be noted that this electronic structure analysis is not intended to be quantitative. On the other hand, it is aimed at characterizing electronic features that correlate with observed surface

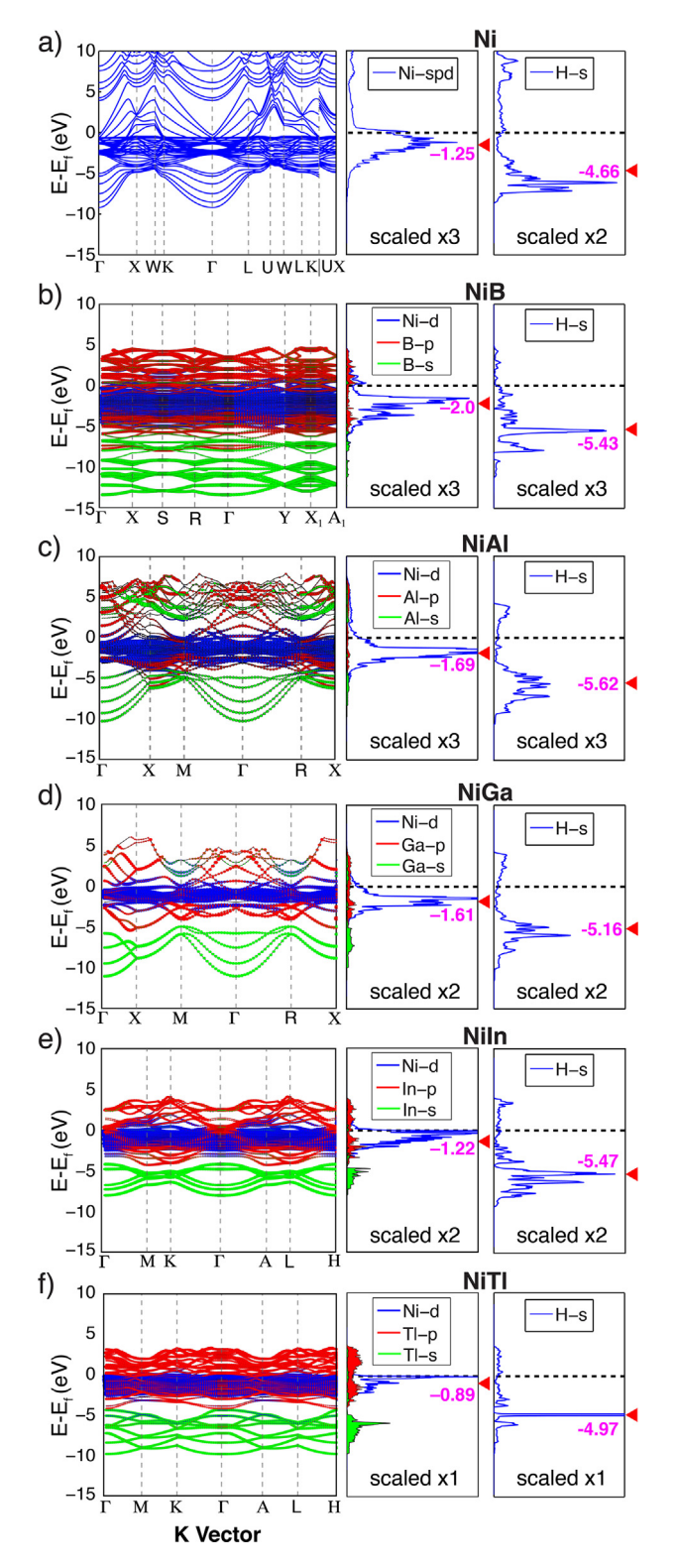


Fig. 4. Electronic analysis of Ni and Ni + B-group IMCs from left to right: band structure and DOS of clean surfaces and DOS of adsorbed atomic H over Ni and Ni + B-group IMCs. Vertically materials are listed as (a) Ni, (b) NiB, (c) NiAl, (d) NiGa, (e) NiIn, and f) NiTI. D-band centers of clean surfaces and s-centers of adsorbed atomic H are indicated by red triangles to the right of the DOS plots. To make the DOS comparisons more facile, DOS were normalized by number of electrons present and scaled. Scaling is noted in each plot box.

and catalytic chemistry. In the end, these observations promoted a more in-depth electronic analysis of key adsorbates, namely ethylene and atomic H, to understand how IMC electronic structure

dictates activity in a key selectivity turning point as well as the departures from metal-like BEP correlations for hydrogenation kinetics.

An electronic analysis of adsorbed ethylene and atomic H over Ni and the Ni + B-group IMCs illustrated that specific types of bonding disruption within the adsorbed ethylene as well as the nature of the bond between atomic H and the surface dictate the calculated kinetics. Within the ethylene adsorbate, disruption of the pi bonding/antibonding states occurs universally over all surfaces, as expected, yet new and energetically localized carbonsurface states occur only over NiIn and NiTl (see Fig. 5). The disruption of the pi bonding states may prime the molecule for sigma bond addition through hydrogenation. However, this is dependent upon the ability of the surface to transfer hydrogen. Analysis of the center of the s-state of adsorbed atomic H illustrates a clear connection between lower energy s-centers and limited hydrogenation and vice versa (see Fig. 4). The s-centers track from least to most negative as Ni < NiTl < NiGa < NiB < NiIn < NiAl. Contrasting Ni, NiGa, and NiAl in ethylene hydrogenation, a clear correlation with atomic H electronic state energy and hydrogenation are evident, e.g., Ni > NiGa > NiAl. This was a trend not captured well with the energetics of surface chemical reactivity markers. The elevated s-center energy of atomic H over Ni and NiTl correlates well with more facile hydrogenation throughout the entire reaction mechanism. Focusing upon cases where ethylene adsorption leads to carbon-surface states near the Fermi level, e.g., over NiIn and NiTl, we find this feature leads to C-C bond disruption and more facile C-C coupling. Correlation between kinetics and the degree of disruption in the sigma bonding network within adsorbed ethylene was much less clear, yet suggested another degree of adsorbate activation that may be correlated with reaction pathway preference. The effect of p-element electronegativity in dictating the position of the s-state of atomic H leads to generally limited

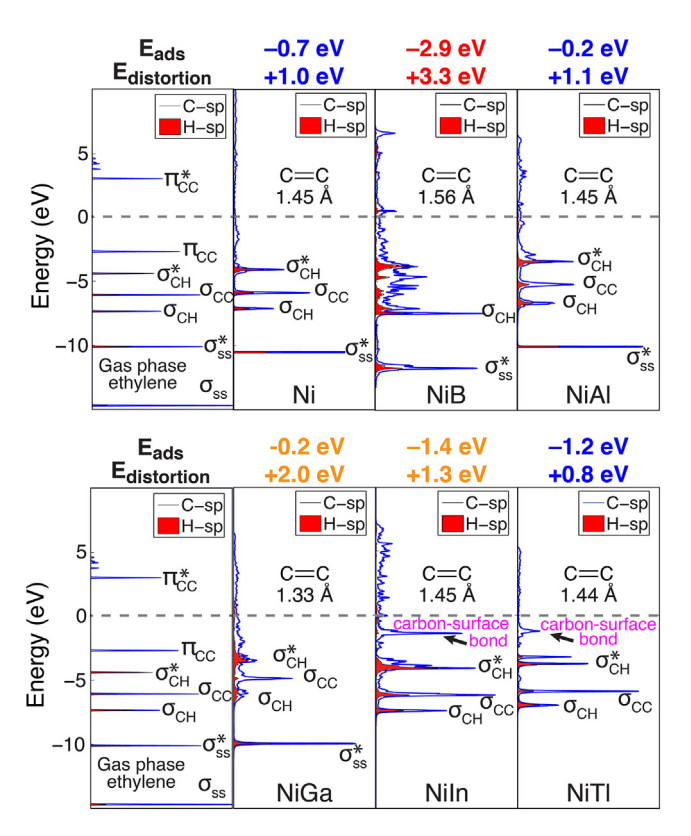


Fig. 5. Molecular orbital analysis of ethylene adsorption utilizing gas phase ethylene symmetry designations throughout to ease comparison to the gas phase.

hydrogenation kinetics over the IMCs in comparison to Ni. This feature may be useful to further manipulate the stability of atomic H and its transfer to surface-bound intermediates. These results suggest that electronic analysis of adsorbates may be necessary to fully understand how IMC surface chemistry is produced.

4.3. Effect of XC functionals

The effect of exchange-correlation functional choice on the results derived herein was investigated by recalculating all energetics with PBE, RPBE and PW91 in addition to PBE-sol, PBE-sol has been shown to treat the more localized and hybridized bonding within semiconductors greatly improving the accuracy of calculated band gaps in comparison to PBE, RPBE, or PW91 [62,86–88]. Because the bonding within the IMCs varies considerably depending upon the p-element selection and exhibited a range of metallic and more hybridized bonding characteristics, use of the PBE-sol functional may produce more realistic results on a case-by-case basis. It should be stated that PBE-sol has been noted to suffer inaccuracy in capturing the bonding within isolated molecules, which translates to a small degree of error in the calculation of adsorption energies [139-142]. Because adsorption/desorption is unlikely to dramatically affect the major pathways of interest, these errors are unlikely to affect conclusions drawn. However, it was important to investigate the reaction energetics of surface reactions to determine whether error induced by the functional would affect conclusions (see Table S12).

In general, marginal changes were found in reaction energetics as the XC functional was modified. Select thermodynamic energetics were affected to a greater degree, but, interestingly, calculated kinetic barriers were generally within a few tenths of an eV leaving conclusions unmodified. On a material-specific basis, both thermodynamic energies and kinetic barriers calculated using PBE-sol deviated most significantly from PBE, RPBE, and PW91 when modeling the solids that exhibited more hybridized/covalent bonding, namely NiB, NiAl, and NiGa (strict covalent bonding is not implied). Because of markedly varying bulk bonding nature and a lack of experimental and computational surface science studies to compare with, it is still unclear which XC functional is most accurate for IMCs or if it is IMC specific. These same trends were found in our studies of compounds of Ti or Ni bound with the nonmetals and their surface and catalytic chemistry in the deoxygenation of a woody biomass model compound [43,44].

5. Conclusions

In conclusion, our studies presented herein have helped to shed some direction on how constituent element selection, orbital overlap, bulk bonding, and reaction site composition systematically dictate the surface and catalytic chemistry of TM IMCs in the semi-hydrogenation of acetylene. Results demonstrate that the nature of the electronic structure of the Ni + B-group IMCs transforms from moderately hybridized (NiB) to highly hybridized (NiAl and NiGa) back to moderately hybridized (NiIn and NiTl) as a function of the Ni-p-element orbital overlap. The changes in the nature of the bulk bonding of the IMCs also translates to markedly manipulated surface chemistry towards C=C bonds and significantly modulates hydrogenation activity. Changes in IMC bulk bonding also produced a full spectrum of surface chemical traits that would be characterized as electronic and ensemble-like depending on the contribution of the surface p-elements to the observed surface chemistry. New BEP correlations are also evident over the Ni + Bgroup IMCs that exhibit strong electronic effects and pronounced p-element contributions to the surface chemistry. Correlations of hydrogenation thermodynamics and kinetics over these materials (NiB, NiAl, and NiGa) depart significantly from the trends observed over monometallic TM surfaces suggesting that new and unique control of catalytic chemistry is possible through the new electronic structures presented by select IMCs. The new surface chemistry encountered over the IMCs also necessitated an in-depth electronic analysis of both the IMCs and the critical adsorbates ethylene and atomic H to understand the trends in reaction energetics. Analysis of the disruption of molecular orbitals within adsorbed ethylene and the center of the s-state for adsorbed atomic H with respect to the Fermi level provided additional markers that tracked well with observed hydrogenation kinetics of ethylene. In the end, the observations made in this study suggest that the surface chemistry of IMCs may be abundantly tunable beyond simple physical ensemble effects and may be made to present wholly unique surface chemistry towards unsaturated C—C bonds and modified hydrogenation activity that has heretofore been mostly inaccessible over monometallic TMs. TM + TM alloys, and TM + CM IMCs and alloys. An IMC compositional space where size match of constituent elements improves orbital overlap and significantly modifies surface and catalytic chemistry has also been identified.

Acknowledgments

This research was supported by the National Science Foundation (NSF) CAREER award (Grant CBET-1752063) and the American Chemical Society Petroleum Research Fund (Grant PRF# 57589-ND5). This work used the Extreme Science and Engineering Discovery Environment (XSEDE), which is supported by the National Science Foundation (Project: TG-CTS140009).

Appendix A. Supplementary material

Supplementary data associated with this article can be found, in the online version, at https://doi.org/10.1016/j.jcat.2019.02.018.

References

- [1] I. Amghizar, L.A. Vandewalle, K.M. Van Geem, G.B. Marin, New trends in olefin production, Engineering 3 (2) (2017) 171–178, https://doi.org/10.1016/j. eng.2017.02.006.
- [2] F. Studt, F. Abild-Pedersen, T. Bligaard, R.Z. Sorensen, C.H. Christensen, J.K. Nørskov, Identification of non-precious metal alloy catalysts for selective hydrogenation of acetylene, Science 320 (5881) (2008) 1320–1322, https:// doi.org/10.1126/science.1156660.
- [3] E.W. Shin, C.H. Choi, K.S. Chang, Y.H. Na, S.H. Moon, Properties of Si-modified Pd catalyst for selective hydrogenation of acetylene, Catal. Today 44 (1-4) (1998) 137–143, https://doi.org/10.1016/s0920-5861(98)00184-9.
- [4] J. Chen, B. Fruhberger, Similarities in the decomposition and dehydrogenation of cyclohexene on (4 × 4)-C/Mo(110) and Pt(111), Surf. Sci. 367 (1996) L102– L110, https://doi.org/10.1016/S0039-6028(96)00993-4.
- [5] F. Besenbacher, Design of a surface alloy catalyst for steam reforming, Science 279 (5358) (1998) 1913–1915, https://doi.org/ 10.1126/science.279.5358.1913.
- [6] K. Tomishige, K. Asakura, Y. Iwasawa, Design and characterization by EXAFS, FTIR, and TEM of Rh-Sn/SiO₂ catalysts active for NO-H₂ reaction, J. Catal. 149 (1) (1994) 70–80, https://doi.org/10.1006/jcat.1994.1273.
- [7] M. Garcia-Mota, B. Bridier, J. Perez-Ramirez, N. Lopez, Interplay between carbon monoxide, hydrides, and carbides in selective alkyne hydrogenation on palladium, J. Catal. 273 (2) (2010) 92–102, https://doi.org/10.1016/j. jcat.2010.04.018.
- [8] T. Komatsu, S. Hyodo, T. Yashima, Catalytic properties of Pt–Ge intermetallic compounds in the hydrogenation of 1,3-butadiene, J. Phys. Chem. B 101 (28) (1997) 5565–5572, https://doi.org/10.1021/jp9711171.
- [9] B. Riguetto, C. Rodrigues, M. Morales, E. Baggio-Saitovitch, L. Gengembre, E. Payen, C. Marques, J. Bueno, Ru-Sn catalysts for selective hydrogenation of crotonaldehyde: effect of the Sn/(Ru+Sn) ratio, Appl. Catal. A: General 318 (2007) 70–78, https://doi.org/10.1016/j.apcata.2006.10.045.
- [10] Rodiansono, S. Khairi, T. Hara, N. Ichikuni, S. Shimazu, Highly efficient and selective hydrogenation of unsaturated carbonyl compounds using Ni–Sn alloy catalysts, Catal. Sci. Technol. 2 (10) (2012) 2139, https://doi.org/ 10.1039/c2cy20216f.
- [11] F. Seyedeyn-Azad, E. Salehi, J. Abedi, T. Harding, Biomass to hydrogen via catalytic steam reforming of bio-oil over Ni-supported alumina catalysts, Fuel

- Process. Technol. 92 (3) (2011) 563–569, https://doi.org/10.1016/i.fuproc.2010.11.012.
- [12] G.W. Huber, Raney Ni-Sn catalyst for H₂ production from biomass-derived hydrocarbons, Science 300 (5628) (2003) 2075–2077, https://doi.org/ 10.1126/science.1085597.
- [13] S. Poudyal, S. Laursen, Insights into elevated-temperature photocatalytic reduction of CO₂ by H₂O, J. Phys. Chem. C 122 (15) (2018) 8045–8057, https://doi.org/10.1021/acs.jpcc.7b12662.
- [14] A. Gutierrez, R. Kaila, M. Honkela, R. Slioor, A. Krause, Hydrodeoxygenation of guaiacol on noble metal catalysts, Catal. Today 147 (3-4) (2009) 239–246, https://doi.org/10.1016/j.cattod.2008.10.037.
- [15] Y.-C. Lin, C.-L. Li, H.-P. Wan, H.-T. Lee, C.-F. Liu, Catalytic hydrodeoxygenation of guaiacol on Rh-based and sulfided CoMo and NiMo catalysts, Energy Fuels 25 (3) (2011) 890–896, https://doi.org/10.1021/ef101521z.
- [16] P.M. de Souza, R.C. Rabelo-Neto, L.E.P. Borges, G. Jacobs, B.H. Davis, U.M. Graham, D.E. Resasco, F.B. Noronha, Effect of zirconia morphology on hydrodeoxygenation of phenol over Pd/ZrO₂, ACS Catal. 5 (12) (2015) 7385–7398, https://doi.org/10.1021/acscatal.5b01501.
- [17] C.A. Teles, R.C. Rabelo-Neto, J.R. de Lima, L.V. Mattos, D.E. Resasco, F.B. Noronha, The effect of metal type on hydrodeoxygenation of phenol over silica supported catalysts, Catal. Lett. 146 (10) (2016) 1848–1857, https://doi.org/10.1007/s10562-016-1815-5.
- [18] D. Gao, C. Schweitzer, H.T. Hwang, A. Varma, Conversion of guaiacol on noble metal catalysts: reaction performance and deactivation studies, Ind. Eng. Chem. Res. 53 (49) (2014) 18658–18667, https://doi.org/10.1021/ie500495z.
- [19] T. Mochizuki, S. Chen, M. Toba, Y. Yoshimura, Deoxygenation of guaiacol and woody tar over reduced catalysts, Appl. Catal. B: Environ. 146 (2014) 237– 243, https://doi.org/10.1016/j.apcatb.2013.05.040.
- [20] C.-C. Chang, C.-H. Yeh, J.-J. Ho, Theoretical study of selective hydrogenation in a mixture of acetylene and ethylene over Fe@W(111) bimetallic surfaces, Appl. Catal. A: General 462–463 (2013) 296–301, https://doi.org/10.1016/j. apcata.2013.05.014.
- [21] J. Zhou, Y. Yang, C. Li, S. Zhang, Y. Chen, S. Shi, M. Wei, Synthesis of Co-Sn intermetallic nanocatalysts toward selective hydrogenation of citral, J. Mater. Chem. A 4 (33) (2016) 12825–12832, https://doi.org/10.1039/c6ta04542a.
- [22] D.-M. Rao, S.-T. Zhang, C.-M. Li, Y.-D. Chen, M. Pu, H. Yan, M. Wei, The reaction mechanism and selectivity of acetylene hydrogenation over Ni-Ga intermetallic compound catalysts: a density functional theory study, Dalton Trans. 47 (12) (2018) 4198–4208, https://doi.org/10.1039/c7dt04726f.
- [23] L. Piccolo, L. Kibis, The partial hydrogenation of butadiene over Al₁₃Fe₄: a surface-science study of reaction and deactivation mechanisms, J. Catal. 332 (2015) 112–118, https://doi.org/10.1016/j.jcat.2015.09.018.
- [24] A. Onda, T. Komatsu, T. Yashima, Characterization and catalytic properties of Ni–Sn intermetallic compounds in acetylene hydrogenation, Phys. Chem. Chem. Phys. 2 (13) (2000) 2999–3005, https://doi.org/10.1039/b0013811.
- [25] A. Onda, T. Komatsu, T. Yashima, Characterizations and catalytic properties of fine particles of Ni–Sn intermetallic compounds supported on SiO₂, J. Catal. 221 (2) (2004) 378–385, https://doi.org/10.1016/j.jcat.2003.08.012.
- [26] C. Li, Y. Chen, S. Zhang, J. Zhou, F. Wang, S. He, M. Wei, D. Evans, X. Duan, Nickel-gallium intermetallic nanocrystal catalysts in the semihydrogenation of phenylacetylene, ChemCatChem 6 (3) (2014) 824–831, https://doi.org/ 10.1002/cctc.201300813.
- [27] C. Li, Y. Chen, S. Zhang, S. Xu, J. Zhou, F. Wang, M. Wei, D.G. Evans, X. Duan, Ni-In intermetallic nanocrystals as efficient catalysts toward unsaturated aldehydes hydrogenation, Chem. Mater. 25 (19) (2013) 3888–3896, https:// doi.org/10.1021/cm4021832.
- [28] H. Li, H. Yang, H. Li, Highly active mesoporous Co–B amorphous alloy catalyst for cinnamaldehyde hydrogenation to cinnamyl alcohol, J. Catal. 251 (1) (2007) 233–238, https://doi.org/10.1016/j.jcat.2007.07.022.
- [29] T. Komatsu, T. Kishi, T. Gorai, Preparation and catalytic properties of uniform particles of Ni₃Ge intermetallic compound formed inside the mesopores of MCM-41, J. Catal. 259 (2) (2008) 174–182, https://doi.org/10.1016/j. icat.2008.08.001.
- [30] T. Komatsu, M. Fukui, T. Yashima, Cobalt intermetallic compounds for selective hydrogenation of acetylene, Stud. Surf. Sci. Catal. (1996) 1095– 1104. https://doi.org/10.1016/s0167-2991(96)80321-1.
- [31] X. Chen, M. Li, J. Guan, X. Wang, C.T. Williams, C. Liang, Nickel-silicon intermetallics with enhanced selectivity in hydrogenation reactions of cinnamaldehyde and phenylacetylene, Ind. Eng. Chem. Res. 51 (9) (2012) 3604–3611, https://doi.org/10.1021/ie202227j.
- [32] M. Armbrüster, M. Behrens, F. Cinquini, K. Föttinger, Y. Grin, A. Haghofer, B. Klötzer, A. Knop-Gericke, H. Lorenz, A. Ota, S. Penner, J. Prinz, C. Rameshan, Z. Révay, D. Rosenthal, G. Rupprechter, P. Sautet, R. Schlögl, L. Shao, L. Szentmiklosi, D. Teschner, D. Torres, R. Wagner, R. Widmer, G. Wowsnick, How to control the selectivity of palladium-based catalysts in hydrogenation reactions: The role of subsurface chemistry, ChemCatChem 4 (8) (2012) 1048–1063, https://doi.org/10.1002/cctc.201200100.
- [33] J. Gao, H. Zhao, X. Yang, B.E. Koel, S.G. Podkolzin, Controlling acetylene adsorption and reactions on Pt-Sn catalytic surfaces, ACS Catal. 3 (6) (2013) 1149-1153, https://doi.org/10.1021/cs400198f.
- [34] Q. Feng, S. Zhao, Y. Wang, J. Dong, W. Chen, D. He, D. Wang, J. Yang, Y. Zhu, H. Zhu, et al., Isolated single-atom Pd sites in intermetallic nanostructures: high catalytic selectivity for semihydrogenation of alkynes, J. Am. Chem. Soc. 139 (21) (2017) 7294–7301, https://doi.org/10.1021/jacs.7b01471.
- [35] K. Kovnir, J. Osswald, M. Armbruster, D. Teschner, G. W, U. Wild, A. Knop-Gericke, T. Ressler, Y. Grin, R. Schlogl, Etching of the intermetallic compounds

- PdGa and Pd_3Ga_7 : an effective way to increase catalytic activity?, J Catal. 264 (2) (2009) 93–103, https://doi.org/10.1016/j.jcat.2009.03.007.
- [36] M. Armbrüster, K. Kovnir, M. Behrens, D. Teschner, Y. Grin, R. Schlögl, Pd–Ga intermetallic compounds as highly selective semihydrogenation catalysts, J. Am. Chem. Soc. 132 (42) (2010) 14745–14747, https://doi.org/10.1021/ja106568t.
- [37] Y. Chen, J. Chen, Selective hydrogenation of acetylene on SiO₂ supported Ni-In bimetallic catalysts: promotional effect of In, Appl. Surf. Sci. 387 (2016) 16– 27, https://doi.org/10.1016/j.apsusc.2016.06.067.
- [38] J. Shabaker, D. Simonetti, R. Cortright, J. Dumesic, Sn-modified Ni catalysts for aqueous-phase reforming: characterization and deactivation studies, J. Catal. 231 (1) (2005) 67–76, https://doi.org/10.1016/j.jcat.2005.01.019.
- [39] A. García-Trenco, A. Regoutz, E.R. White, D.J. Payne, M.S. Shaffer, C.K. Williams, PdIn intermetallic nanoparticles for the hydrogenation of CO₂ to methanol, Appl. Catal. B: Environ. 220 (2018) 9–18, https://doi.org/10.1016/j.apcatb.2017.07.069.
- [40] T. Komatsu, M. Mesuda, T. Yashima, Aromatization of butane on Pt-Ge intermetallic compounds supported on HZSM-5, Appl. Catal. A: General 194-195 (2000) 333–339, https://doi.org/10.1016/s0926-860x(99)00379-8.
- [41] Y. Cao, Z. Sui, Y. Zhu, X. Zhou, D. Chen, Selective hydrogenation of acetylene over Pd-In/Al₂O₃ catalyst: promotional effect of indium and compositiondependent performance, ACS Catal. 7 (11) (2017) 7835–7846, https://doi.org/ 10.1021/acscatal.7b01745.
- [42] Y. He, Y. Song, D.A. Cullen, S. Laursen, Selective and stable non-noble-metal intermetallic compound catalyst for the direct dehydrogenation of propane to propylene, J. Am. Chem. Soc. 140 (43) (2018) 14010–14014, https://doi.org/ 10.1021/jacs.8b05060.
- [43] Y. He, S. Laursen, Trends in the surface and catalytic chemistry of transition-metal ceramics in the deoxygenation of a woody biomass pyrolysis model compound, ACS Catal. 7 (5) (2017) 3169–3180, https://doi.org/10.1021/acscatal.6b02806.
- [44] Y. He, S. Laursen, The surface and catalytic chemistry of the first row transition metal phosphides in deoxygenation, Catal. Sci. Technol. 8 (20) (2018) 5302–5314, https://doi.org/10.1039/c8cy01134f.
- [45] P. Bechthold, M. Sandoval, E.A. González, G. Brizuela, A. Bonivardi, P.V. Jasen, The electronic structure and bonding of acetylene on PdGa(110), J. Phys. Chem. C 119 (32) (2015) 18229–18238, https://doi.org/10.1021/acs. ipcc.5b04214.
- [46] J. Shabaker, G. Huber, J. Dumesic, Aqueous-phase reforming of oxygenated hydrocarbons over Sn-modified Ni catalysts, J. Catal. 222 (1) (2004) 180–191, https://doi.org/10.1016/j.jcat.2003.10.022.
- [47] M. Krajci, J. Hafner, The (210) surface of intermetallic B20 compound GaPd as a selective hydrogenation catalyst: a DFT study, J. Catal. 295 (2012) 70–80, https://doi.org/10.1016/j.jcat.2012.07.025.
- [48] M. Krajci, J. Hafner, Intermetallic compound AlPd as a selective hydrogenation catalyst: a DFT study, J. Phys. Chem. C 116 (10) (2012) 6307–6319, https://doi.org/10.1021/jp212317u.
- [49] M. Krajci, J. Hafner, Semihydrogenation of acetylene on the (010) surface of GaPd₂: Ga enrichment improves selectivity, J. Phys. Chem. C 118 (23) (2014) 12285–12301, https://doi.org/10.1021/jp5025075.
- [50] M. Krajci, J. Hafner, Complex intermetallic compounds as selective hydrogenation catalysts – a case study for the (100) surface of Al₁₃Co₄, J. Catal. 278 (2) (2011) 200–207, https://doi.org/10.1016/j.jcat.2010.12.004.
- [51] M. Meier, J. Ledieu, V. Fournée, É. Gaudry, Semihydrogenation of acetylene on Al₅Co₂ surfaces, J. Phys. Chem. C 121 (9) (2017) 4958–4969, https://doi.org/ 10.1021/acs.jpcc.6b11083.
- [52] Y. Liu, X. Liu, Q. Feng, D. He, L. Zhang, C. Lian, R. Shen, G. Zhao, Y. Ji, D. Wang, G. Zhou, Y. Li, Intermetallic Ni_xM_y (M = Ga and Sn) nanocrystals: a non-precious metal catalyst for semi-hydrogenation of alkynes, Adv. Mater. 28 (23) (2016) 4747–4754.
- [53] J. Prinz, C.A. Pignedoli, Q.S. Stöckl, M. Armbrüster, H. Brune, O. Gröning, R. Widmer, D. Passerone, Adsorption of small hydrocarbons on the three-fold PdGa surfaces: the road to selective hydrogenation, J. Am. Chem. Soc. 136 (33) (2014) 11792–11798, https://doi.org/10.1021/ja505936b.
- [54] M. Krajčí, J. Hafner, Selective semi-hydrogenation of acetylene: Atomistic scenario for reactions on the polar threefold surfaces of GaPd, J. Catal. 312 (2014) 232–248, https://doi.org/10.1016/j.jcat.2014.02.001.
- [55] M. Krajčí, J. Hafner, Intermetallic compounds as selective heterogeneous catalysts: insights from DFT, ChemCatChem 8 (1) (2015) 34–48, https://doi. org/10.1002/cctc.201500733.
- [56] A. Dannenberg, M.E. Gruner, A. Hucht, P. Entel, Surface energies of stoichiometric FePt and CoPt alloys and their implications for nanoparticle morphologies, Phys. Rev. B 80 (24) (2009), https://doi.org/10.1103/physrevb.80.245438.
- [57] M. Krajčí, J. Hafner, Surfaces of intermetallic compounds: an ab initio DFT study for B20-type AlPd, Phys. Rev. B 87 (3) (2013), https://doi.org/ 10.1103/physrevb.87.035436.
- [58] A.H. Haner, P.N. Ross, U. Bardi, A. Atrei, Surface composition determination of Pt-Sn alloys by chemical titration with carbon monoxide, J. Vac. Sci. Technol. A: Vacuum, Surf., Films 10 (4) (1992) 2718–2722, https://doi.org/10.1116/ 1577964
- [59] P. Haas, F. Tran, P. Blaha, Calculation of the lattice constant of solids with semilocal functionals, Phys. Rev. B 79 (8) (2009), https://doi.org/ 10.1103/physrevb.79.085104.
- [60] J.A. Abraham, G. Pagare, S.S. Chouhan, S.P. Sanyal, Theoretical calculations of structural, electronic, optical, elastic, and thermal properties of YX₃ (X = In, Sn, Tl, and Pb) compounds based on density functional theory, J. Mater. Sci. 50 (2) (2014) 542–554, https://doi.org/10.1007/s10853-014-8610-8.

- [61] S. Bhatt, K. Kumar, G. Arora, K. Bapna, B. Ahuja, High energy compton spectroscopy and electronic structure of laves phase ZrFe₂, Radiat. Phys. Chem. 125 (2016) 109–114, https://doi.org/10.1016/j. radphyschem.2016.03.021.
- [62] J.P. Perdew, A. Ruzsinszky, G.I. Csonka, O.A. Vydrov, G.E. Scuseria, L.A. Constantin, X. Zhou, K. Burke, Restoring the density-gradient expansion for exchange in solids and surfaces, Phys. Rev. Lett. 100 (13) (2008), https://doi.org/10.1103/physrevlett.100.136406.
- [63] F. Zegrar, S. Boucetta, B. Othmani, High pressure behaviour of elastic and mechanical properties of NiGa intermetallic compound, Acta Phys. Pol., A 130 (1) (2016) 471–474, https://doi.org/10.12693/aphyspola.130.471.
- [64] K. Sharma, J. Sahariya, B. Ahuja, Electronic structure, optical properties and compton profiles of RuO₂: performance of PBEsol exchange-correlation approximation, J. Alloy. Compd. 645 (2015) 414-420, https://doi.org/ 10.1016/j.jallcom.2015.05.117.
- [65] A. Bouhemadou, S. Al-Essa, D. Allali, M. Ghebouli, S. Bin-Omran, Electronic and optical properties of ZnSc₂S₄ and CdSc₂S₄ cubic spinels by the modified Becke–Johnson density functional, Solid State Sci. 20 (2013) 127–134, https:// doi.org/10.1016/j.solidstatesciences.2013.03.016.
- [66] R.-P. Blum, D. Ahlbehrendt, H. Niehus, Preparation-dependent surface composition and structure of NiAl(001): SPA-LEED and NICISS study, Surf. Sci. 366 (1) (1996) 107–120, https://doi.org/10.1016/0039-6028(96)00782-0.
- [67] L. Hammer, H. Graupner, V. Blum, K. Heinz, G. Ownby, D. Zehner, Segregation phenomena on surfaces of the ordered bimetallic alloy FeAl, Surf. Sci. 412-413 (1998) 69–81, https://doi.org/10.1016/s0039-6028(98)00370-7.
- [68] J. Osswald, R. Giedigkeit, R. Jentoft, M. Armbrüster, F. Girgsdies, K. Kovnir, T. Ressler, Y. Grin, R. Schlögl, Palladium-gallium intermetallic compounds for the selective hydrogenation of acetylene part I: preparation and structural investigation under reaction conditions, J. Catal. 258 (1) (2008) 210–218, https://doi.org/10.1016/j.jcat.2008.06.013.
- [69] A. Moscu, Y. Schuurman, L. Veyre, C. Thieuleux, F. Meunier, Direct evidence by in situ IR CO monitoring of the formation and the surface segregation of a Pt-Sn alloy, Chem. Commun. 50 (62) (2014) 8590, https://doi.org/10.1039/ c4c03208i.
- [70] C. Rameshan, W. Stadlmayr, S. Penner, H. Lorenz, L. Mayr, M. Hävecker, R. Blume, T. Rocha, D. Teschner, A. Knop-Gericke, R. Schlögl, D. Zemlyanov, M. Norbert, B. Klötzer, In situ XPS study of methanol reforming on PdGa near-surface intermetallic phases, J. Catal. 290 (2012) 126–137, https://doi.org/10.1016/j.jcat.2012.03.009.
- [71] H. Brongersma, M. Draxler, M. Deridder, P. Bauer, Surface composition analysis by low-energy ion scattering, Surf. Sci. Rep. 62 (3) (2007) 63–109, https://doi.org/10.1016/j.surfrep.2006.12.002.
- [72] M.J. Gladys, F. Samavat, B.V. King, D.J. O'Connor, Modeling and measurement of Al interlayer diffusion in Pd(100): a low-energy ion scattering study, Phys. Rev. B 69 (16) (2004), https://doi.org/10.1103/physrevb.69.165418.
- [73] V. Matoli'n, I. Matoli'nová, F. Šutara, K. Veltruská, Co interaction with Ni₃Al alloy: XPS, LEIS and TPD study, Surf. Sci. 566–568 (2004) 1093–1096, https://doi.org/10.1016/j.susc.2004.06.057.
- [74] D.C. Nerko, S. Axnanda, J.C. Lofaro, W.-P. Zhou, M.G. White, Synthesis and characterization of surface oxide films on CoGa(100), Surf. Sci. 616 (2013) 192–197, https://doi.org/10.1016/j.susc.2013.06.003.
- [75] W. Priyantha, R. Droopad, M. Kopczyk, R. Smith, A. Kayani, Structure of V thin films on Al(100) using XPD, LEED, and LEIS, Surf. Sci. 606 (15-16) (2012) 1160-1166, https://doi.org/10.1016/j.susc.2012.03.012.
- [76] F. Qin, J. Anderegg, C. Jenks, B. Gleeson, D. Sordelet, P. Thiel, The effect of Pt on Ni₃Al surface oxidation at low-pressures, Surf. Sci. 601 (1) (2007) 146–154, https://doi.org/10.1016/j.susc.2006.09.014.
- [77] M. Benam, N. Abdoshahi, M. Majidiyan Sarmazdeh, Ab initio study of the effect of pressure on the structural and electronic properties of cubic LaAlO₃ by density function theory using GGA, LDA and PBEsol exchange correlation potentials, Physica B 446 (2014) 32–38, https://doi.org/10.1016/j.physb.2014.04.006.
- [78] B. Zhang, Y. Duan, K. Johnson, Density functional theory study of CO₂ capture with transition metal oxides and hydroxides, J. Chem. Phys. 136 (6) (2012) 064516, https://doi.org/10.1063/1.3684901.
- [79] A. Ruzsinszky, G.I. Csonka, G.E. Scuseria, Regularized gradient expansion for atoms, molecules, and solids, J. Chem. Theory Comput. 5 (4) (2009) 763–769, https://doi.org/10.1021/ct8005369.
- [80] G.I. Csonka, J.P. Perdew, A. Ruzsinszky, P.H.T. Philipsen, S. Lebègue, J. Paier, O. A. Vydrov, J.G. Ángyán, Assessing the performance of recent density functionals for bulk solids, Phys. Rev. B 79 (15) (2009), https://doi.org/10.1103/physrevb.79.155107.
- [81] G. Kresse, D. Joubert, From ultrasoft pseudopotentials to the projector augmented-wave method, Phy. Rev. B 59 (3) (1999) 1758–1775, https://doi. org/10.1103/physrevb.59.1758.
- [82] G. Kresse, J. Furthmüller, Efficient iterative schemes for ab initio total-energy calculations using a plane-wave basis set, Phys. Rev. B 54 (16) (1996) 11169– 11186, https://doi.org/10.1103/physrevb.54.11169.
- [83] G. Kresse, J. Furthmüller, Efficiency of ab-initio total energy calculations for metals and semiconductors using a plane-wave basis set, Comput. Mater. Sci. 6 (1) (1996) 15–50, https://doi.org/10.1016/0927-0256(96)00008-0.
- [84] G. Kresse, J. Hafner, Ab initio molecular dynamics for liquid metals, Phys. Rev. B 47 (1) (1993) 558–561, https://doi.org/10.1103/physrevb.47.558.
- [85] J. Towns, T. Cockerill, M. Dahan, I. Foster, K. Gaither, A. Grimshaw, V. Hazlewood, S. Lathrop, D. Lifka, G.D. Peterson, R. Roskies, J.R. Scott, N. Wilkins-Diehr, XSEDE: accelerating scientific discovery, Computing in

- Science & Engineering. 16 (5) (2014) 62–74, https://doi.org/10.1109/ MCSF 2014 80
- [86] J.P. Perdew, A. Ruzsinszky, G.I. Csonka, O.A. Vydrov, G.E. Scuseria, L.A. Constantin, X. Zhou, K. Burke, Restoring the density-gradient expansion for exchange in solids and surfaces, Phys. Rev. Lett. 102 (3) (2009), https://doi.org/10.1103/PhysRevLett.100.136406.
- [87] E.-E. Castaño-González, N. Seña, V. Mendoza-Estrada, R. González-Hernández, A. Dussan, F. Mesa, First-principles calculations of the electronic and structural properties of GaSb, Semiconductors 50 (10) (2016) 1280–1286, https://doi.org/10.1134/s1063782616100110.
- [88] T. Mahmood, C. Cao, F.K. Butt, H. Jin, Z. Usman, W.S. Khan, Z. Ali, M. Tahir, F. Idrees, M. Ahmed, Elastic, electronic and optical properties of cotunnite TiO₂ from first principles calculations, Physica B 407 (22) (2012) 4495–4501, https://doi.org/10.1016/j.physb.2012.08.006.
- [89] D. Sheppard, P. Xiao, W. Chemelewski, D.D. Johnson, G. Henkelman, A generalized solid-state nudged elastic band method, J. Chem. Phys. 136 (7) (2012) 074103, https://doi.org/10.1063/1.3684549.
- [90] J. Kästner, P. Sherwood, Superlinearly converging dimer method for transition state search, J. Chem. Phys. 128 (1) (2008) 014106, https://doi.org/10.1063/ 1.2815812.
- [91] P. Xiao, D. Sheppard, J. Rogal, G. Henkelman, Solid-state dimer method for calculating solid-solid phase transitions, J. Chem. Phys. 140 (17) (2014) 174104, https://doi.org/10.1063/1.4873437.
- [92] G. Henkelman, H. Jónsson, Improved tangent estimate in the nudged elastic band method for finding minimum energy paths and saddle points, J. Chem. Phys. 113 (22) (2000) 9978, https://doi.org/10.1063/1.1323224.
- [93] C.M. Fang, M.H.F. Sluiter, M.A. van Huis, H.W. Zandbergen, Structural and magnetic properties of NiC_x and NiN_x(x= 0 to 13) solid solutions from firstprinciples calculations, Phys. Rev. B 86 (13) (2012), https://doi.org/ 10.1103/physrevb.86.134114.
- [94] I. Shein, N. Medvedeva, A. Ivanovskii, Electronic and structural properties of cementite-type M3X (M=Fe, Co, Ni; X=C or B) by first principles calculations, Phys. B: Condens Matter 371 (1) (2006) 126–132, https://doi.org/10.1016/ i.physb.2005.10.093.
- [95] L.-S. Hsu, Y.K. Wang, G.Y. Guo, Experimental and theoretical study of the electronic structures of Ni₃Al, Ni₃Ga, Ni₃In, and NiGa, J. Appl. Phys. 92 (3) (2002) 1419–1424, https://doi.org/10.1063/1.1491018.
- [96] P. Mohn, D.G. Pettifor, The calculated electronic and structural properties of the transition-metal monoborides, J. Phys. C: Solid State Phys. 21 (15) (1988) 2829–2839, https://doi.org/10.1088/0022-3719/21/15/015.
- [97] V. Sundararajan, B.R. Sahu, D.G. Kanhere, P.V. Panat, G.P. Das, Cohesive, electronic and magnetic properties of the transition metal aluminides FeAl CoAl and NiAl, J. Phys.: Condens. Matter 7 (30) (1995) 6019–6034, https://doi.org/10.1088/0953-8984/7/30/007.
- [98] C. Deluque Toro, S. Ramos de Debiaggi, A. Monti, Study of cohesive, electronic and magnetic properties of the Ni–In intermetallic system, Physica B 407 (16) (2012) 3236–3239, https://doi.org/10.1016/j.physb.2011.12.075.
- [99] S. Saadi, B. Hinnemann, C.C. Appel, S. Helveg, F. Abild-Pedersen, J.K. Nørskov, First-principles investigations of Ni₃Al(111) and NiAl(110) surfaces at metal dusting conditions, Surf. Sci. 605 (5-6) (2011) 582–592, https://doi.org/ 10.1016/j.susc.2010.12.023.
- [100] B. Hammer, M. Scheffler, Local chemical reactivity of a metal alloy surface, Phys. Rev. Lett. 74 (17) (1995) 3487–3490, https://doi.org/ 10.1103/physrevlett.74.3487.
- [101] G. Jones, J. Jakobsen, S. Shim, J. Kleis, M. Andersson, J. Rossmeisl, F. Abildpedersen, T. Bligaard, S. Helveg, B. Hinnemann, First principles calculations and experimental insight into methane steam reforming over transition metal catalysts, J. Catal. 259 (1) (2008) 147–160, https://doi.org/10.1016/j.jcat.2008.08.003.
- [102] B. Yang, R. Burch, C. Hardacre, G. Headdock, P. Hu, Influence of surface structures, subsurface carbon and hydrogen, and surface alloying on the activity and selectivity of acetylene hydrogenation on Pd surfaces: a density functional theory study, J. Catal. 305 (2013) 264–276, https://doi.org/ 10.1016/j.jcat.2013.05.027.
- [103] Y.-A. Zhu, D. Chen, X.-G. Zhou, W.-K. Yuan, DFT studies of dry reforming of methane on ni catalyst, Catal. Today 148 (3-4) (2009) 260–267, https://doi. org/10.1016/j.cattod.2009.08.022.
- [104] U. Government, National Institute of Standards and Technology.
- [105] L.-L. Ma, C.-Q. Lv, G.-C. Wang, A DFT study and micro-kinetic analysis of acetylene selective hydrogenation on Pd-doped Cu(111) surfaces, Appl. Surf. Sci. 410 (2017) 154–165, https://doi.org/10.1016/j.apsusc.2017.01.084.
- [106] B. Cordero, V. Gómez, A.E. Platero-Prats, M. Revés, J. Echeverría, E. Cremades, F. Barragán, S. Alvarez, Covalent radii revisited, Dalton Trans. (21) (2008) 2832, https://doi.org/10.1039/b801115j.
- [107] G. Hamm, T. Schmidt, J. Breitbach, D. Franke, C. Becker, K. Wandelt, The adsorption of benzene on Pd(111) and ordered Sn/Pd(111) surface alloys, Surf. Sci. 562 (1-3) (2004) 170–182, https://doi.org/10.1016/ i.susc.2004.05.119.
- [108] C. Breinlich, J. Haubrich, C. Becker, A. Valcarcel, F. Delbecq, K. Wandelt, Hydrogenation of 1,3-butadiene on Pd(111) and PdSn/Pd(111) surface alloys under UHV conditions, J. Catal. 251 (1) (2007) 123–130, https://doi.org/ 10.1016/j.jcat.2007.07.003.
- [109] R.D. Cortright, J.M. Hill, J.A. Dumesic, Selective dehydrogenation of isobutane over supported Pt/Sn catalysts, Catal. Today 55 (3) (2000) 213–223, https:// doi.org/10.1016/s0920-5861(99)00249-7.

- [110] Z.-X. Chen, K.M. Neyman, A.B. Gordienko, N. Rösch, Surface structure and stability of PdZn and PtZn alloys: density-functional slab model studies, Phys. Rev. B 68 (7) (2003), https://doi.org/10.1103/physrevb.68.075417.
- [111] H. Zhao, B.E. Koel, Adsorption and reaction of 1,3-butadiene on Pt(111) and Sn/Pt(111) surface alloys, Surf. Sci. 572 (2-3) (2004) 261–268, https://doi. org/10.1016/j.susc.2004.08.039.
- [112] C. Xu, Y.L. Tsai, B.E. Koel, Adsorption of cyclohexane and benzene on ordered tin/platinum (111) surface alloys, J. Phys. Chem. 98 (2) (1994) 585–593, https://doi.org/10.1021/j100053a038.
- [113] K. Brandt, M.E. Chiu, D.J. Watson, M.S. Tikhov, R.M. Lambert, Chemoselective catalytic hydrogenation of acrolein on Ag(111): Effect of molecular orientation on reaction selectivity, J. Am. Chem. Soc. 131 (47) (2009) 17286–17290, https://doi.org/10.1021/ja9063469.
- [114] C. Fan, Y.-A. Zhu, X.-G. Zhou, Z.-P. Liu, Catalytic hydrogenation of benzene to cyclohexene on Ru(0001) from density functional theory investigations, Catal. Today 160 (1) (2011) 234–241, https://doi.org/10.1016/j.cattod.2010.03.075.
- [115] Y. Li, Z. Liu, S.P. Crossley, F.C. Jentoft, S. Wang, Effect of hydrogen coverage on hydrogenation of o-cresol on Pt(111), Appl. Surf. Sci. 443 (2018) 575–580, https://doi.org/10.1016/j.apsusc.2018.02.288.
- [116] C. Rudolf, B. Dragoi, A. Ungureanu, A. Chirieac, S. Royer, A. Nastro, E. Dumitriu, NiAl and CoAl materials derived from takovite-like ldhs and related structures as efficient chemoselective hydrogenation catalysts. Catal. Sci. Technol. 4 (1) (2014) 179–189, https://doi.org/10.1039/c3cy00611e.
- [117] J. Rodríguez, A. Marchi, A. Borgna, A. Monzón, Effect of Zn content on catalytic activity and physicochemical properties of Ni-based catalysts for selective hydrogenation of acetylene, J. Catal. 171 (1) (1997) 268–278, https://doi.org/ 10.1006/jcat.1997.1815.
- [118] L. Baijun, L. Lianhai, W. Bingchun, C. Tianxi, K. Iwatani, Liquid phase selective hydrogenation of furfural on Raney nickel modified by impregnation of salts of heteropolyacids, Appl. Catal. A: General 171 (1) (1998) 117–122, https:// doi.org/10.1016/s0926-860x(98)00081-7.
- [119] Rodiansono, T. Hara, N. Ichikuni, S. Shimazu, A novel preparation method of Ni–Sn alloy catalysts supported on aluminium hydroxide: application to chemoselective hydrogenation of unsaturated carbonyl compounds, Chem. Lett. 41 (8) (2012) 769–771, https://doi.org/10.1246/cl.2012.769.
- [120] F. Devred, A. Gieske, N. Adkins, U. Dahlborg, C. Bao, M. Calvo-Dahlborg, J. Bakker, B. Nieuwenhuys, Influence of phase composition and particle size of atomised Ni–Al alloy samples on the catalytic performance of Raney-type nickel catalysts, Appl. Catal. A: General 356 (2) (2009) 154–161, https://doi.org/10.1016/j.apcata.2008.12.039.
- [121] T. Harada, M. Yamamoto, S. Onaka, M. Imaida, H. Ozaki, A. Tai, Y. Izumi, The enantioface-differentiating (asymmetric) hydrogenation of the C=O double bond with modified Raney nickel. XXXVI. the development of modified nickel catalysts with high enantioface-differentiating abilities, Bull. Chem. Soc. Jpn. 54 (8) (1981) 2323–2329, https://doi.org/10.1246/bcsj.54.2323.
- [122] A. Tai, T. Kikukawa, T. Sugimura, Y. Inoue, T. Osawa, S. Fujii, Highly efficient enantio-differentiating hydrogenation over an ultrasonicated raney nickel catalyst modified with tartaric acid, J. Chem. Soc., Chem. Commun. 0 (12) (1991) 795, https://doi.org/10.1039/c39910000795.
- [123] C.S. Spanjers, J.T. Held, M.J. Jones, D.D. Stanley, R.S. Sim, M.J. Janik, R.M. Rioux, Zinc inclusion to heterogeneous nickel catalysts reduces oligomerization during the semi-hydrogenation of acetylene, J. Catal. 316 (2014) 164–173, https://doi.org/10.1016/j.jcat.2014.05.007.
- [124] S.-J. Chiang, C.-H. Yang, Y.-Z. Chen, B.-J. Liaw, High-active nickel catalyst of NiB/SiO₂ for citral hydrogenation at low temperature, Appl. Catal. A: General 326 (2) (2007) 180–188, https://doi.org/10.1016/j.apcata.2007.04.019.
- [125] Y.-Z. Chen, B.-J. Liaw, S.-J. Chiang, Selective hydrogenation of citral over amorphous NiB and CoB nano-catalysts, Appl. Catal. A: General 284 (1-2) (2005) 97-104, https://doi.org/10.1016/j.apcata.2005.01.023.
- [126] J. Choi, N.M. Yoon, An excellent nickel boride catalyst for the cis-selective semihydrogenation of acetylenes, Tetrahedron Lett. 37 (7) (1996) 1057– 1060, https://doi.org/10.1016/0040-4039(95)02347-x.

- [127] Y. Nitta, T. Imanaka, S. Teranishi, Partial hydrogenation of acetylenes on modified nickel boride catalysts, Bull. Chem. Soc. Jpn. 54 (11) (1981) 3579– 3580, https://doi.org/10.1246/bcsj.54.3579.
- [128] B.-J. Liaw, S.-J. Chiang, S.-W. Chen, Y.-Z. Chen, Preparation and catalysis of amorphous CoNiB and polymer-stabilized CoNiB catalysts for hydrogenation of unsaturated aldehydes, Appl. Catal. A: General 346 (1-2) (2008) 179–188, https://doi.org/10.1016/j.apcata.2008.05.025.
- [129] J.A. Schreifels, P.C. Maybury, W.E. Swartz, Comparison of the activity and lifetime of Raney nickel and nickel boride in the hydrogenation of various functional groups, J. Organic Chem. 46 (7) (1981) 1263–1269, https://doi.org/ 10.1021/jo00320a008.
- [130] Y. Jin, A.K. Datye, E. Rightor, R. Gulotty, W. Waterman, M. Smith, M. Holbrook, J. Maj, J. Blackson, The influence of catalyst restructuring on the selective hydrogenation of acetylene to ethylene, J. Catal. 203 (2) (2001) 292–306, https://doi.org/10.1006/jcat.2001.3347.
- [131] R. Alcala, J.W. Shabaker, G.W. Huber, M.A. Sanchez-Castillo, J.A. Dumesic, Experimental and DFT studies of the conversion of ethanol and acetic acid on PtSn-based catalysts†, J. Phys. Chem. B 109 (6) (2005) 2074–2085, https://doi. org/10.1021/jp049354t.
- [132] L. Luo, Z. Duan, H. Li, J. Kim, G. Henkelman, R.M. Crooks, Tunability of the adsorbate binding on bimetallic alloy nanoparticles for the optimization of catalytic hydrogenation, J. Am. Chem. Soc. 139 (15) (2017) 5538–5546, https://doi.org/10.1021/jacs.7b01653.
- [133] A.J. Medford, A. Vojvodic, J.S. Hummelshøj, J. Voss, F. Abild-Pedersen, F. Studt, T. Bligaard, A. Nilsson, J.K. Nørskov, From the sabatier principle to a predictive theory of transition-metal heterogeneous catalysis, J. Catal. 328 (2015) 36– 42, https://doi.org/10.1016/j.jcat.2014.12.033.
- [134] S. Wang, V. Petzold, V. Tripkovic, J. Kleis, J.G. Howalt, E. Skúlason, E.M. Fernández, B. Hvolbæk, G. Jones, A. Toftelund, et al., Universal transition state scaling relations for (de)hydrogenation over transition metals, Phys. Chem. Chem. Phys. 13 (46) (2011) 20760, https://doi.org/10.1039/c1cp20547a.
- [135] J.R. Kitchin, J.K. Nørskov, M.A. Barteau, J.G. Chen, Trends in the chemical properties of early transition metal carbide surfaces: a density functional study, Catal. Today 105 (1) (2005) 66–73, https://doi.org/10.1016/ i.cattod.2005.04.008.
- [136] M. Armbrüster, K. Kovnir, M. Friedrich, D. Teschner, G. Wowsnick, M. Hahne, P. Gille, L. Szentmiklósi, M. Feuerbacher, M. Heggen, et al., Al₁₃Fe₄ as a low-cost alternative for palladium in heterogeneous hydrogenation, Nat. Mater. 11 (8) (2012) 690–693, https://doi.org/10.1038/nmat3347.
- [137] D. Shi, B. Wen, R. Melnik, S. Yao, T. Li, First-principles studies of Al-Ni intermetallic compounds, J. Solid State Chem. 182 (10) (2009) 2664–2669, https://doi.org/10.1016/j.jssc.2009.07.026.
- [138] G.P. Das, B.K. Rao, P. Jena, S.C. Deevi, Electronic structure of substoichiometric Fe-Al intermetallics, Phys. Rev. B 66 (18) (2002), https://doi.org/10.1103/physrevb.66.184203.
- [139] J. Sun, M. Marsman, A. Ruzsinszky, G. Kresse, J.P. Perdew, Improved lattice constants, surface energies, and CO desorption energies from a semilocal density functional, Phys. Rev. B 83 (12) (2011), https://doi.org/ 10.1103/physrevb.83.121410.
- [140] L. Schimka, J. Harl, G. Kresse, Improved hybrid functional for solids: the HSEsol functional, J. Chem. Phys. 134 (2) (2011) 024116, https://doi.org/ 10.1063/1.3524336.
- [141] L. Schimka, J. Harl, A. Stroppa, A. Grüneis, M. Marsman, F. Mittendorfer, G. Kresse, Accurate surface and adsorption energies from many-body perturbation theory, Nat. Mater. 9 (9) (2010) 741–744, https://doi.org/10.1038/nmat2806.
- [142] M. Bajdich, J.K. Nørskov, A. Vojvodic, Surface energetics of alkaline-earth metal oxides: trends in stability and adsorption of small molecules, Phys. Rev. B 91 (15) (2015). https://doi.org/10.1103/physrevb.91.155401.